

计算机辅助在 TKY 管节点焊缝超声相控阵检测中的应用

陆铭慧, 程 俊, 邵红亮, 孙明磊

(南昌航空大学 无损检测技术教育部重点实验室, 南昌 330063)

摘 要: 采用解析几何理论与方法, 对 TKY 管节点焊缝进行了数学模型的构建. 在获得管节点焊缝截面图形基础上, 按照规定尺寸绘制焊缝接头, 并依据实物尺寸绘制相控阵探头轮廓和超声波的声束线. 运用计算机辅助技术实现了焊接接头声束覆盖范围可视化效果, 较好地指导了相控阵检测工艺设计, 能够对 TKY 管节点焊缝超声检测盲区进行评估, 从而克服了相控阵超声检测参数设置的盲目性. 对人工设计的 Y 形管节点焊缝试样检测表明, 利用超声相控阵成像技术和计算机辅助技术相结合手段有助于管节点焊缝作快速检测和评价.

关键词: TKY 管节点; 超声相控阵; 计算机辅助; 声束覆盖

中图分类号: TG115.28 **文献标识码:** A **文章编号:** 0253-360X(2012)04-0045-04



陆铭慧

0 序 言

TKY 管节点是空间钢网结构中最重要和最常见的结构形式. 目前, 对于管节点焊缝主要采用横波斜探头进行检测, 由于其声束折射角度单一, 一次和二次声波尚不能较好的覆盖焊接接头区域, 导致产生较大的检测盲区. 不同管节点焊缝位置其盲区大小也不能有效地进行评估. 加之常规超声波检测存在反射波识别困难、缺陷定位方法复杂、探头折射角度选择繁琐、缺陷当量误差大等问题. 其中缺陷定位的方法是管节点焊缝探伤的关键. 为检测此类焊缝, 现多采用作图分析法、声程修正法对缺陷定位^[1]. 作图分析法由于原理简单, 能够直观确定缺陷位置, 达到缺陷定位要求, 故普遍被大家应用, 但由于其作图工作量大, 缺陷定位效率低下, 管节点焊缝超声探伤人为因素造成误差较大等缺点制约了作图分析法在实际检测中的应用.

随着科学技术不断发展和新型技术的广泛应用, 焊缝检测正朝着超声波成像和计算机辅助方向发展. 相控阵技术运用于超声检测, 可以解决复杂类构件和难以接近工件的检测问题. TKY 管节点焊缝就属于此类问题, 相控阵超声检测技术的介入对解决此问题提供了技术支持. 运用计算机辅助方法

可实现超声相控阵扫查声束在管节点焊缝接头处的覆盖效果, 可以有效地评价焊缝接头的盲区大小, 并可以根据超声相控阵检测设备提供的数据对缺陷进行评定^[2].

1 管节点焊缝模型

刘兴亚等人^[3]通过数学推导, 建立了 TKY 管节点焊缝各结构参数的相互关系, 采用计算机辅助计算, 绘制了几何临界角与相贯角、声程修正系数及水平距离修正系数与相贯角和偏角的关系曲线. 赵志斌^[4]对比已有的探伤方法, 改进已有的数学模型, 提出合理性的简化思想, 以管节点中最具有代表性的 Y 形管节点作为研究对象, 建立了 Y 形管节点的数学几何模型. 文中在改进的管节点数学模型基础上, 建立 TKY 焊缝接头模型, 并仿真超声相控阵声束覆盖焊缝接头.

1.1 焊缝接头模型的建立

超声波束截交管节点焊缝剖面图形如图 1 所示. 焊缝宽度为 n , 根部间隙为 m ; 主管椭圆中心点为 O_2 ; 支管椭圆中心点为 O_1 , 两椭圆短轴的夹角为 λ , 建立平面直角坐标系, 定义 O_1 为坐标原点, 支管长轴方向为 x 方向, 支管短轴方向为 y 方向, 支管椭圆方程表示为

$$\frac{x^2}{a^2} + \frac{y^2}{b^2} = 1 \quad (1)$$

主管椭圆经过坐标旋转、平移,方程可表示为^[4]

$$\frac{(x \cos \lambda - \gamma y \sin \lambda - x_2 \cos \lambda + \gamma y_2 \sin \lambda)^2}{a^2} + \frac{(\gamma x \sin \lambda + y \cos \lambda - \gamma x_2 \sin \lambda - y_2 \cos \lambda)^2}{b^2} = 1 \quad (2)$$

式中: a b 分别为所在椭圆的长短轴; x_2 y_2 为 O_2 坐标; γ 为椭圆旋转系数,根据椭圆旋转方式不同其取值为 ± 1 .

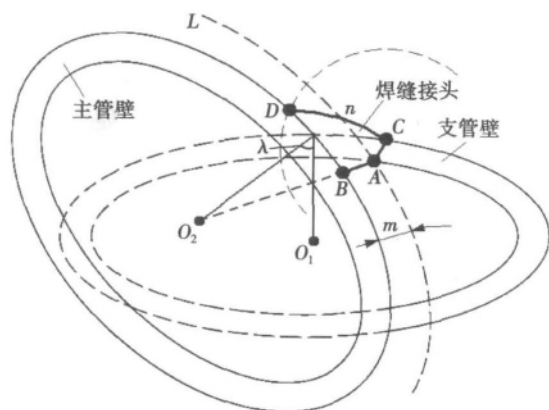


图1 管节点焊缝截面

Fig. 1 Cross-section of tubular joint weld

为确定预留为 m 的根部间隙位置,以 O_2 为圆心,作一条平行于主管外壁的椭圆曲线 L ,曲线 L 与支管内壁交于点 A . 直线连接 A 点与 O_2 点,交主管外壁于点 B ,线段 AB 即为间隙所在位置.

焊缝坡口角度根据美国石油协会 API 标准^[1],当二面角度小于 20° 时,支管不开坡口;二面角介于 $20^\circ \sim 30^\circ$ 时,支管坡口角度 $\phi = 15^\circ$;二面角介于 $30^\circ \sim 90^\circ$ 时,支管坡口角度 ϕ 为二面角度的一半;二面角度大于 90° 时,支管坡口角度 $\phi = 45^\circ$. 直线 AC 与曲线 L 在 A 点的切线夹角为支管所开坡口角度,根据平面直角坐标系中两直线的夹角公式,坡口直线的斜率为 k_{AC} . 联立直线 AC 方程与支管外壁椭圆方程,可以确定 C 点坐标. 圆心为 C ,半径为 n 的圆交主管外壁于点 D ,根据二分查找法^[5] D 点坐标可以确定.

直线连接点 A B C ,曲线连接点 C 与点 D . 至此管节点焊缝任意位置处焊缝接头模型建立完成.

1.2 相控阵声束线确定

为确定相控阵声束线在管节点焊缝覆盖情况,现固定相控阵探头在支管处位置,如图2所示. 定义阵元所在位置坐标为 $E(x_e, y_e)$,阵元距离探头底面高度为 h ,相控阵探头底面直线斜率为 k ,入射角为 α 的声束以折射角度 β 进入支管壁,入射角与折射角满足折射定理. 根据几何关系,可以确定声束

入射点 R 的坐标为

$$\left. \begin{aligned} x_R &= x_e - \frac{h}{\cos \alpha} \cos\left(\frac{\pi}{2} + \arctan k - \alpha\right) \\ y_R &= y_e - \frac{h}{\cos \alpha} \sin\left(\frac{\pi}{2} + \arctan k - \alpha\right) \end{aligned} \right\} \quad (3)$$

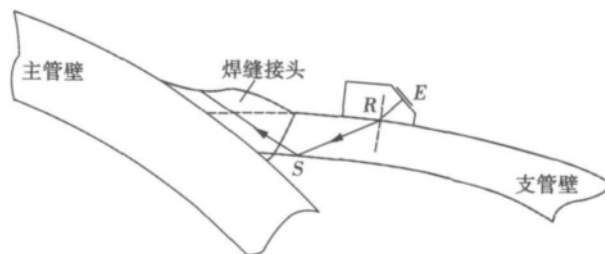


图2 声束入射焊缝接头示意图

Fig. 2 Schematic of acoustic beam in weld joints

声束入射支管内壁椭圆,与支管内壁交点为 S ,根据声束直线方程与支管内壁椭圆方程联立可以确定 S 点坐标. 声束在支管内壁 S 点反射,其反射线关于 S 点处法线对称,至此声束反射线方程确定.

为更好拟合实际焊缝情况,焊缝接头模型可做人为修正. 默认为标准规定的参数.

2 计算机辅助算法实现

2.1 设计依据

TKY 管节点常规超声检测存在较大盲区,影响缺陷检出率,威胁工业生产安全. 超声相控阵技术扇形扫查方式在管节点焊缝上的运用,可以减少探头在支管外壁的移动,同时多角度的电子扫描缩小了管节点焊接接头的检测盲区. 相控阵扇扫虽具有上述优势,但相控阵超声束覆盖管接头范围仍缺少可视化特点. 相控阵探头在管节点支管壁处具体位姿^[6]及声束扫描范围现多靠检测人员经验确定,这对相控阵检测管节点工艺设计是不利的. 计算机辅助建立在管节点焊缝接头数学模型基础上,计算声束线辐射范围,达到声束可视化目的.

2.2 试验试样与检测设备

试验采用最具代表性的 Y 形管节点为研究对象,材料为 Q235 钢管. 横波声速为 $3\,233$ m/s. 实测主管外径为 218 mm,支管外径为 168 mm,主管交叉角度为 60° ,主管壁厚为 10.6 mm,支管壁厚为 9.06 mm.

超声相控阵试验采用频率 4 MHz,16 阵元,间距为 0.5 mm 探头;横波楔块倾角 36° ,中心阵元高度为 10.6 mm,声速为 $2\,337$ m/s,最大偏转范围标称值为 $30^\circ \sim 70^\circ$.

2.3 分区与声束覆盖

将支管外圆周等分 12 等份,并分别向管端作管轴平行线,交于焊缝根部 12 个点.以管节点脚尖处为 0:00,脚跟处为 6:00,以时钟指针转动为序,分别标记各钟点时刻.运用计算机辅助声束覆盖程序,在各钟点处绘制焊缝截面,并调整相控阵探头位置及声束绘制角度,使声束最佳覆盖管节点焊缝接头,覆盖效果如图 3 所示.

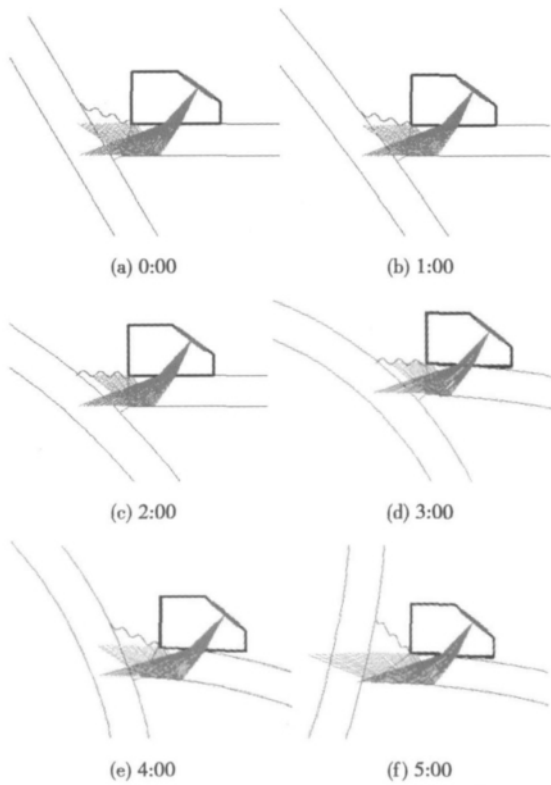


图 3 各钟点焊缝截面声束覆盖效果

Fig. 3 Effect of weld cross-section beam coverage at each clock time

图 3a~3f 中,探头距焊缝边缘距离为 0 mm,扇形扫描角度为 $35^{\circ} \sim 70^{\circ}$,即可最大范围覆盖管接头焊缝区域.根据各钟点焊缝扇扫声束覆盖情况,设置相控阵检测设备扇扫偏转角度为 $30^{\circ} \sim 70^{\circ}$ (此范围稍大于程序仿真范围),探头紧靠焊缝边缘扫描即可满足管节点焊缝检测盲区最小要求.

3 试验分析

为实现程序对焊缝中可疑信号的定位,文中采用管节点结构回波和自然缺陷作为定位对象.

3.1 伪缺陷识别

主管内壁的反射回波属于结构回波,在检测过

程中需对此类信号进行识别,避免参与缺陷的判定,其产生是由于主声束透过焊缝垂直入射到主管内壁的反射回波.现选取试验中两组主管内壁反射回波对其具体反射点进行定位,如表 1 所示.

表 1 主管内壁反射点位置

Table 1 Internal wall reflection position of main pipe

编号	相贯角 $\varphi/(^{\circ})$	扫描线角度 $\beta/(^{\circ})$	声程 w/mm	备注
1	112.5	61.2	24.3	一次波
2	166.4	59.6	32.5	二次波

相控阵扇扫图形如图 4 所示,图 4a 为一次声波经焊缝区域入射主管内壁扇扫图形,图 4b 为声束经支管内壁反射后,二次波束经焊缝区域入射主管内壁扇扫图形.

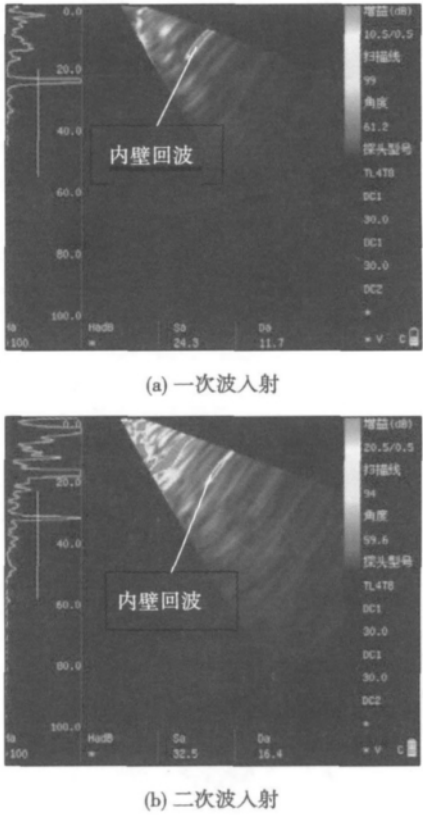


图 4 相控阵扇扫图像

Fig. 4 Phased array sector scanning image

主管内壁回波由于其特征是回波波幅极高,故在增益一定时,内壁回波扇扫成像表现出明显的色差.为确定其信号来源,采用计算机辅助方法定位,如图 5 所示.图 5 中程序根据扫描线角度及回波声程,可以确定信号的反射点均来自于主管内壁.其中 D_0 为反射点距焊缝边缘垂直距离; w 为反射波声程; Y_0 为声束入射点距焊缝边缘弧长.从声束终

点位置可以确定缺陷信号的来源。

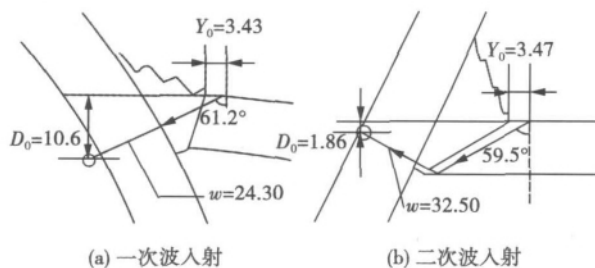


图 5 结构波计算机辅助定位图 (mm)

Fig. 5 Structure echoes computer-aided positioning

3.2 缺陷定位

实际检测过程中除需对结构回波(内壁回波、焊道回波、根部反射波等)进行识别外,更多是对缺陷信号进行标定。对试样焊接产生的自然缺陷检测结果如表 2 所示。计算机辅助定位如图 6 所示。

表 2 缺陷位置
Table 2 Defect position

	声束入射点距焊缝 边缘弧长 Y_0 / mm	反射点距焊缝 边缘垂直距离 D_0 / mm
作图解析法	19.5	7.0
计算机辅助	18.91	7.38
相对误差	3.03%	5.43%

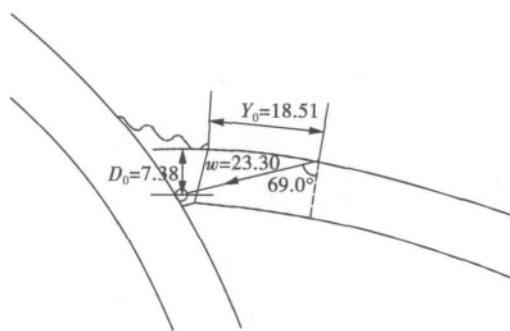


图 6 缺陷波计算机辅助定位图 (mm)

Fig. 6 Flaw echo computer-aided positioning

表 2 得出了计算机辅助定位与作图解析法定位的误差值。相对误差在 5% 左右。两种定位方法数据差异小于 1 mm。表明计算机辅助定位在一定程度上有利于对缺陷快速定位,提高检测效率。

图 5、图 6 中,计算机辅助程序根据检测过程中确定的声束角度及声程,自动标定反射点位置。根据以上试验数据分析,在利用超声相控阵技术检测管节点焊缝过程中,可以借助计算机辅助手段识别伪缺陷信号,并对管节点缺陷位置进行标定。计算

机辅助定位前提是对管结构原始尺寸准确测量,这些尺寸的误差容易导致缺陷的误判。在保证管节点尺寸精确的情况下,定位误差可以控制在极小范围,这对管壁较薄的管节点焊缝定位是有利的。

4 结 论

(1) 管节点焊缝结构特殊,属于声输入口受到限制的场所,采用超声相控阵扇形扫查可以减小管接头焊缝检测盲区,很大程度上降低了缺陷漏检概率。

(2) 焊缝截面声束覆盖程序可以有效指导相控阵检测工艺的设计,直观显示超声波束在管接头覆盖状态,克服相控阵超声检测参数设置的盲目性。

(3) 基于“作图解析法”缺陷定位程序有利于伪缺陷信号的识别,一定程度上可以满足缺陷定位要求,有助于提高 TKY 管节点检测效率。

(4) 声束截面形状和缺陷评价结果有赖于对原始管节点结构的测量,测量误差仍是影响探伤结果的重要因素之一。

参考文献:

- [1] 程志虎. TKY 管节点焊缝超声波探伤——第一讲 技术特征与影响因素[J]. 无损检测, 1994, 16(8): 234-240.
Cheng Zhihu. Ultrasonic testing of the welds in TKY nodes: characteristics and effect factors [J]. Nondestructive Testing, 1994, 16(8): 234-240.
- [2] 单宝华, 欧进萍. 海洋平台结构管节点焊缝超声相控阵检测技术[J]. 焊接学报, 2004, 25(6): 35-37.
Shan Baohua, Ou Jinping. Ultrasonic phased array inspection technology of offshore platform structure tubular joint welds [J]. Transactions of the China Welding Institution, 2004, 25(6): 35-37.
- [3] 刘兴亚, 晋青珍, 申献辉. TKY 管节点焊缝超声波探伤的计算机辅助计算[J]. 钢结构, 1998, 13(4): 19-23.
Liu Xingya, Jin Qingzhen, Shen Xianhui. Computer aid calculation and its application in the ultrasonic testing for tubular weld of TKY connections [J]. Steel Construction, 1998, 13(4): 19-23.
- [4] 赵志斌. Y 形管节点的超声检测研究[D]. 南京: 南京航空航天大学, 2006.
- [5] 徐士良. 常用算法程序集(C++语言描述)[M]. 北京: 清华大学出版社, 2009.
- [6] 郝广平, 邓宗全. 相控阵探头扫查器检测管节点焊缝的位姿[J]. 焊接学报, 2006, 27(2): 23-26.
Hao Guangping, Deng Zongquan. Pose of ultrasonic phased array scanner in inspecting tubular joint welds [J]. Transactions of the China Welding Institution, 2006, 27(2): 23-26.

作者简介: 陆铭慧, 女, 1963 年出生, 博士, 副教授。主要从事无损检测方面的科研和教学工作。发表论文 20 余篇。Email: lunara@163.com

Study on sub-arc X-ray welding image defect segmentation algorithm and defect model

GAO Weixin¹, HU Yuheng², MU Xiangyang¹, WANG Zhi³ (1. Shanxi Key Laboratory of Oil-Drilling Rigs Controlling Technique, Xi'an Shiyou University, Xi'an 710065, China; 2. Department of Electrical & Computer Engineering, University of Wisconsin-Madison, Madison 53705, USA; 3. National Laboratory of Industrial Control Technology, Zhejiang University, Hangzhou 310027, China). pp 37-41

Abstract: Regarding the present problems that the traditional image segmentation algorithm can only achieve a low successful defect segmentation ratio for the strong noise and low contrast of submerged-arc x-ray image, an efficient X-ray radiography image analysis algorithm is developed for the task of segmentation of submerged-arc welding defects. In the new algorithm, the defect is treated as noise and a new concept—"gray density" is put forward for calculation convenience. Tested with 100 X-ray radiography images obtained from a real factory, the proposed algorithm can increase successful segmentation ratio and achieves a successful ration of 95%. Based on the clustering segmentation algorithm, a high dimension space defect mathematical model is presented. The model makes the characteristic of the complexity of the form into consideration. Real examples show that the model is effective and practical. The sensitivity curve of the presented clustering segmentation algorithm is also given.

Key words: welding gap; defect; segmentation; clustering

Spontaneous growth of Sn whiskers on surface of Sn-Zn-Ga-Pr solders

YE Huan^{1,2}, XUE Songbai¹, XUE Peng¹, CHEN Cheng¹ (1. College of Materials Science and Technology, Nanjing University of Aeronautics and Astronautics, Nanjing 210016, China; 2. Center for Advanced Life Cycle Engineering, University of Maryland, College Park 20742, USA). pp 42-44

Abstract: In spite of many beneficial effects obtained from the doping of rare earth (RE) to lead-free solders, it is newly found that an exceeded addition of RE would cause a risk of Sn whisker growth in the alloys. The results indicate that with the addition of 0.7% Pr to Sn-9Zn-0.5Ga solder, many Sn whiskers spontaneously grow from the surface of Sn-Pr phases in the bulk solder exposed for 12 hours only. And the whiskers show a continuous growth with the exposure time being increased. The final longest length of the whisker can reach 100 μm , which can lead to a serious reliability problem for electronic assemblies. Finally, the mechanical reason for whisker growth is discussed.

Key words: lead-free solder; rare earth; Sn whisker; driving force

Application of computes-aided ultrasonic phased array in inspection of weld in TKY tubular node

LU Minghui, CHENG Jun, SHAO Hongliang, SUN Minglei (Key Lab of Non-destructive Testing, Ministry of Education, Nanchang Hangkong University, Nanchang 330063, China). pp 45-48

Abstract: Analytic geometry theories and methods were applied to found the mathematical model of welds in TKY tubular node. According to the regulation of the size, welded joints were

drawn after getting weld cross-section in tubular node. The ultrasonic phased array probe profile was designed on the basis of its physical size, and ultrasonic beam was also designed. The computer-aided technology can achieve the beam coverage of welded joints, which can commendably guide the design of ultrasonic phased array inspection and evaluate ultrasonic test blind areas of weld in TKY tubular node. The blindness of setting parameters can be overcome in the course of ultrasonic phased array inspection. Tests of weld in artificial Y tubular node indicated that the combination of ultrasonic phased array imaging technology and computer-aided techniques contributed to rapid detection and evaluation of weld in tubular node.

Key words: TKY tubular joint; ultrasonic phased array; computer-aided; beam coverage

Microstructure of TiAl joints brazed with TiNiB high-temperature filler metal

YANG Zhenwen, ZHANG Lixia, XUE Qing, HE Peng (State Key Lab of Advanced Welding and Joining, Harbin Institute of Technology, Harbin 150001, China). pp 49-52

Abstract: High-temperature filler metal of TiNiB prepared by arc melting was used as an active filler metal in vacuum brazing of TiAl alloy. The effect of brazing temperature on the microstructure evolution of the joints was studied in this paper. The TiNiB filler metal was mainly comprised of TiNi and TiNi₃ eutectic microstructure, in which some TiB₂ blocks appeared. The melting point of the filler metal was 1 120 °C. The dissolution of TiAl substrate has a strong effect on interfacial structure. The TiAl alloy adjacent to brazed seam was transformed to β layer with the dissolution of TiAl substrate. The microstructure of the brazed seam was comprised of Ti-Al-Ni compounds and a little β phase. TiB₂ was transformed to TiB due to the reaction with Ti.

Key words: TiAl alloy; TiNiB filler; brazing; microstructure

Investigation on wear resistance of Fe-based composite material containing titanium

ZONG Lin^{1,2}, LIU Zhengjun¹, LI Lecheng¹ (1. School of Material Science and Engineering, Shenyang University of Technology, Shenyang 110178, China; 2. School of Mechanical Engineering, Shenyang University of Chemical Technology, Shenyang 110142, China). pp 53-56

Abstract: A series of Fe-Cr-Ti-C hardfacing alloys with different Cr contents were prepared by PTA in order to develop a Fe-based wear resistant composite material. The microstructure and carbides morphology were investigated by means of scanning electron microscopy (SEM) and X-ray diffraction (XRD). The results show that the matrix transforms from austenite and ferrite to ferrite and martensite, the volume fraction of M_7C_3 and TiC increase with the Cr content being increased. In addition, the effects of Cr content on wear resistance were studied. The wear resistance of cladding layer increases with increase of Cr content. When Cr content is 20.1%, the microstructure characteristic with a high volume fraction of hexagonal M_7C_3 complex carbides and a small amount globular, exploded and agglomerated TiC particles are distributed in the lath martensite matrix with higher strength and toughness, which suggests that the cladding layer has a excellent wear resistance.